

Steered Molecular Dynamics Studies of Titin I1 Domain Unfolding

Mu Gao,* Matthias Wilmanns,[†] and Klaus Schulten*

*Department of Physics and Beckman Institute, University of Illinois, Urbana, Illinois 61801 USA and [†]EMBL Hamburg Outstation, D-22603 Hamburg, Germany

ABSTRACT The cardiac muscle protein titin, responsible for developing passive elasticity and extensibility of muscle, possesses about 40 immunoglobulin-like (Ig) domains in its I-band region. Atomic force microscopy (AFM) and steered molecular dynamics (SMD) have been successfully combined to investigate the reversible unfolding of individual Ig domains. However, previous SMD studies of titin I-band modules have been restricted to I27, the only structurally known Ig domain from the distal region of the titin I-band. In this paper we report SMD simulations unfolding I1, the first structurally available Ig domain from the proximal region of the titin I-band. The simulations are carried out with a view toward upcoming atomic force microscopy experiments. Both constant velocity and constant force stretching have been employed to model mechanical unfolding of oxidized I1, which has a disulfide bond bridging β -strands C and E, as well as reduced I1, in which the disulfide bridge is absent. The simulations reveal that I1 is protected against external stress mainly through six interstrand hydrogen bonds between its A and B β -strands. The disulfide bond enhances the mechanical stability of oxidized I1 domains by restricting the rupture of backbone hydrogen bonds between the A' and G-strands. The disulfide bond also limits the maximum extension of I1 to ~ 220 Å. Comparison of the unfolding pathways of I1 and I27 are provided and implications to AFM experiments are discussed.

INTRODUCTION

Titin, ~ 1 μm long, is the longest covalently linked protein known in the human genome (Consortium, 2001). Spanning half of the muscle sarcomere, a single titin molecule extends from the Z disk to the M line through both the A-band and I-band sections of sarcomere. Titin primarily consists of ~ 300 modules in two motif types, immunoglobulin-like (Ig) and fibronectin type III (FnIII) domains. The titin A-band is composed of regular arrangements of these domains that bind to myosin and, hence, cannot be extended upon tension. The titin I-band, however, is extensible and is thought to be responsible for the passive elasticity of muscle (Wang, 1996; Erickson, 1997; Maruyama, 1997; Linke, 2000; Tskhovrebova and Trinick, 2002; Granzier and Labeit, 2002). In cardiac muscle the titin I-band contains four structural units: the proximal Ig region, the N2B or N2BA segment, the PEVK region, and the distal Ig region (Freiburg et al., 2000) (a diagram of titin I-band is shown in Fig. 1 a). The PEVK region contains 163 or more amino acids, 70% of which are proline, glutamate, valine, and lysine. It is a mixture of unstable coiled conformations and polyproline type II helix and easily elongates to develop passive tension under small forces of up to 20 pN (Linke et al., 1998; Trombitas et al., 1998; Ma et al., 2001; Li et al., 2001a). The structure of N2B or N2BA is still unknown. Studies have shown that the N2B segment is critical for reversible extensibility of cardiac myofibrils (Linke et al., 1999). The proximal and distal Ig regions in human cardiac

muscle have 15 and 22 tandem Ig domains, respectively. It has been suggested that some Ig domains unfold to provide extension for the over-stretched muscle (Erickson, 1994; Politou et al., 1995; Granzier et al., 1996; Minajeva et al., 2001).

The reversible unfolding of titin Ig domains has been demonstrated in studies using atomic force microscopy (AFM) and optical tweezers (Rief et al., 1997; Carrion-Vazquez et al., 1999; Kellermayer et al., 1997; Tskhovrebova et al., 1997). The AFM experiments have shown a characteristic sawtooth pattern in force-extension profiles, which can be attributed to the subsequent unraveling of several Ig domains. In order to exclude heterogeneous effects caused by different modules, polyproteins composed of identical I27 or I28 modules were genetically engineered and stretched in AFM experiments (Oberhauser et al., 1999; Marszalek et al., 1999; Li et al., 2000). Analysis of the sawtooth force-extension profiles revealed that the unfolding of domains occurs in two steps within the millisecond timescale: forces of 50–150 pN extend the domains by ~ 7 Å; forces above 150 pN extend the domains further, inducing complete unfolding.

To interpret the AFM experiments at the atomic level, conformational changes of the Ig domains during the unfolding processes must be known. The AFM experiments motivated a series of steered molecular dynamics (SMD) simulations of the unfolding/refolding pathways of the module (Lu et al., 1998; Lu and Schulten, 1999, 2000; Marszalek et al., 1999; Gao et al., 2001), as reviewed in (Isralewitz et al., 2001). The SMD simulations of I27 revealed that the two-step unfolding pathway observed in AFM experiments corresponds to two sequential events of interstrand hydrogen bond rupture, in which two sets of hydrogen bonds connecting β -strands A and B, and β -strands A' and G (see

Submitted May 24, 2002 and accepted for publication September 3, 2002.

Address reprint requests to: Klaus Schulten, University of Illinois at Urbana-Champaign, 405 N. Mathews Ave., Urbana, IL 61801. Tel.: 217-244-1604; Fax: 217-244-6078; E-mail: kschulte@ks.uiuc.edu.

© 2002 by the Biophysical Society

0006-3495/02/12/3435/11 \$2.00

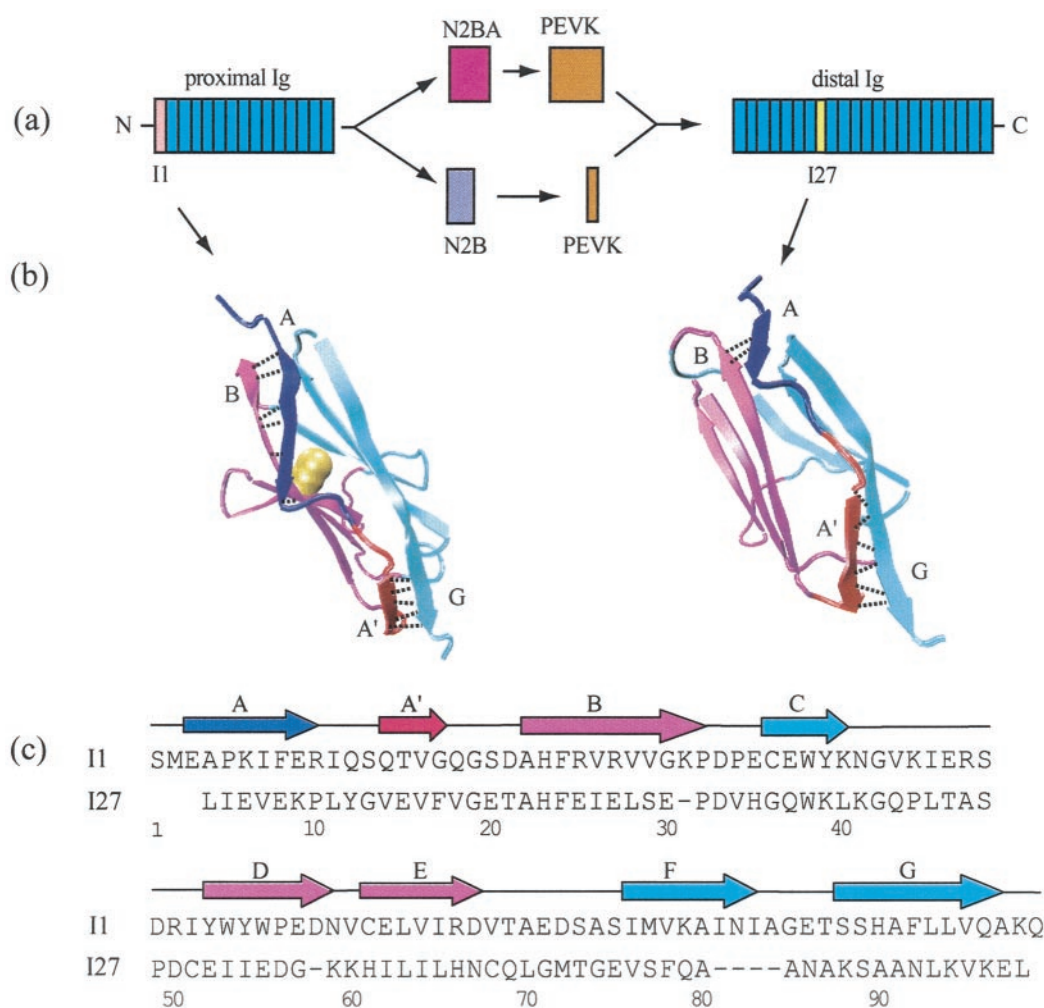


FIGURE 1 (a) Modular structure of the I-band section of cardiac titin. (b) Cartoon representations of the structures of titin I1 (left) and I27 (right) domains. Color scheme: sulfur atoms (yellow), A-strand (blue), A'-strand (red), B-, E-, C-strands (purple), G-, F-, C-, D-strands (cyan). Backbone hydrogen bonds between strands A and B and between A' and G are represented as black dashed lines. (c) Sequence alignment of I1 and I27 domains following Mayans et al. (2001). The secondary structure is shown according to I1.

structure of I27 in Fig. 1b), are broken. At forces around 100 pN the first set of hydrogen bonds near the N-terminus breaks with a concomitant 4- to 7-Å extension, in agreement with the extension-force profile recorded in AFM experiments; the second set of hydrogen bonds breaks at forces of above 200 pN and initiates the complete unfolding (Marszalek et al., 1999). The height of the kinetic barrier separating the folded and unfolded states has been probed in both AFM experiments (Carrion-Vazquez et al., 1999) and SMD simulations (Lu and Schulten, 1999). Moreover, the scenarios of unfolding provided by SMD simulations using explicit solvent models revealed a key role of water molecules: the unfolding barrier is crossed with the help of water molecules that attack interstrand hydrogen bonds (Lu and Schulten, 2000). The competition for hydrogen bond partners with water molecules is also important for the backbone oxygen and hydrogen atoms when they seek to reform

hydrogen bonds in the spontaneous refolding process of I27: by driving water molecules away and reforming six A'-G backbone hydrogen bonds, a stretched I27 domain has been seen to spontaneously refold (Gao et al., 2001).

Alternative simulation approaches have also been carried out by other researchers. Paci and Karplus (1999, 2000) simulated the unfolding of I27 by employing implicit solvent models. Their simulations are computationally less expensive than the simulations based on explicit solvent described above. However, omitting water molecules yields lower force peaks than otherwise. Klimov and Thirumalai (1999) performed simulations using lattice models and off-lattice models (Klimov and Thirumalai, 2000). The latter generated unfolding peak forces of I27 in agreement with the measurements from AFM experiments. Although the correlation between unfolding and the rupture of intrastrand hydrogen bonds could not be established, simulations of

off-lattice models apparently reproduced the same unfolding pathway of I27 as earlier molecular dynamics simulations of all-atom models.

Our previous SMD simulations of titin modules were focused on I27 from the distal Ig region of the titin I-band, until recently the only Ig domain with known structure. The now available crystallographic structure of titin I1 determined at 2.1 Å resolution (Mayans et al., 2001) provides structural information of an Ig domain from the proximal Ig region of titin and a long-awaited opportunity to compare modules from different Ig regions of the titin I-band. The secondary structures and sequences of I1 and I27 are compared in Fig. 1, *b* and *c*. Both modules are built in a motif called β -sandwich, formed by two β -sheets with four β -strands in each sheet. Compared to I27, however, I1 has two features that lead to different mechanical properties. First, I1 has a disulfide bond connecting its C- and E-strands, which restricts the relative movement of the two β -sheets in an oxidizing environment, i.e., when the bond is formed. Since 40% of Ig domains in titin I-band have the potential to form a disulfide bond (Mayans et al., 2001), the role of this bond in protecting the integrity of I1 has general implications to other homologous Ig domains. Second, I1 has more backbone hydrogen bonds between its A- and B-strands than between its A' and G' strands (six versus five), whereas I27 has fewer A-B hydrogen bonds than A'-G hydrogen bonds (two versus six). Previous SMD simulations have shown that the interstrand hydrogen bonding structure of the A-B and the A'-G strand pairs are the key determinant for the mechanical response of I27; one would expect, therefore, to observe a difference in the mechanical function of I1 and I27.

In this paper we present steered molecular dynamics simulations that compare the stretching and unfolding of I1 and I27. We will first describe the modeling and simulation procedure. An analysis of the pattern of interstrand hydrogen bonds will be provided for latter classification of the unfolding pathways of these modules. The implications of the simulation results to upcoming AFM experiments will be discussed.

METHODS

Initial atomic coordinates of the titin I1 domain were taken from the Protein Data Bank (entry code 1G1C; Mayans et al., 2001). Hydrogen atoms were added to the protein using X-PLOR (Brünger, 1992). Cysteine residues, Cys³⁶ and Cys⁶¹, were patched for modeling the disulfide bridge of an oxidized I1 domain, while for modeling a reduced I1 domain the Cys residues were not bonded. A TIP3 water (Jorgensen et al., 1983) sphere of 72 Å diameter was used for solvating the I1 domains, resulting in systems of 18,072 atoms for the oxidized I1 domain and 18,074 atoms for the reduced I1 domain. Fig. 2 shows the model of the oxidized I1 domain. All molecular dynamics simulations were performed using the program NAMD (Kalé et al., 1999) with the CHARMM22 force field (MacKerell Jr., et al., 1998).

Simulations of oxidized and reduced I1 were carried out using the same protocol. First, an I1 system was minimized for 2000 conjugate gradient steps. Following the minimization, the system was heated from 0 K to 300 K in 10 ps and was coupled to a 300 K heat bath for additional 10 ps. The temperature control was released, and the whole system was subsequently

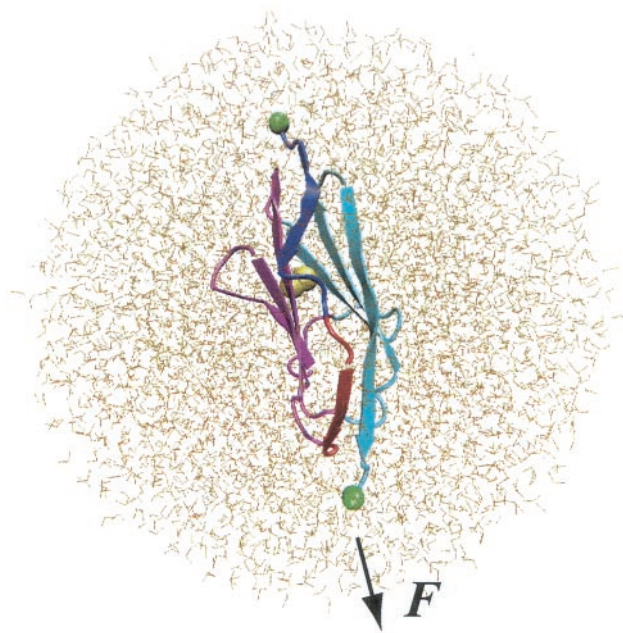


FIGURE 2 Sample system simulated. An oxidized I1 domain was solvated in a water sphere (brown) of 72 Å diameter. The protein was fixed at the N-terminus (green), and external forces were applied to the C-terminus (green).

equilibrated for 1 ns. Finally, SMD simulations were carried out by fixing the C_α atom of the N-terminus of I1 and applying external forces to the C_α atom of the C-terminus. The forces were directed along the vector from the pulled atom to the fixed atom (Fig. 2).

Both constant force and constant velocity protocols were used for the SMD simulations. In the latter case the pulling atom is harmonically constrained with a force $F = -k(x - vt)$, where k is the spring constant, x is the coordinate of the pulling atom, v is the velocity of the atom, and t is the time. The value of k was set to $7 k_B T / \text{Å}^2$, corresponding to a thermal fluctuation of the pulling atom of $\sqrt{k_B T / k} = 0.38 \text{ Å}$. An integration time step of 1 fs and a uniform dielectric constant of 1 were chosen. For calculating electrostatics and van der Waals interactions, a cut-off was employed, switching the interactions smoothly off between 10 Å and 13 Å.

Including simulations of I27 following the same protocol, 14 SMD runs, altogether over 50 ns, were completed using a cluster of 32 1.33-GHz Athlon processors, on which a 1-ns simulation required ~30 h wall clock time. The 14 simulations were carried out under different conditions, e.g., with different values of constant force or with different pulling velocities. These SMD simulations are referred to as cf-SMD (force value) for constant force stretching and cv-SMD (velocity value) for constant velocity stretching.

The analysis of molecular structures and hydrogen bond energies were conducted using X-PLOR and VMD (Humphrey et al., 1996). Atomic coordinates were saved every 1 ps. The coordinates for the pulling atom were saved every 10 fs for cv-SMD simulations and were saved every 100 fs for cf-SMD simulations. The extension of the protein is defined as the change of the end-to-end distance between the two termini. An explicit hydrogen-bonding energy term was used in hydrogen bond energy calculations, with parameters adopted from param11.pro in X-PLOR.

RESULTS

Equilibration

During the 1-ns free dynamics equilibration, both oxidized I1 and reduced I1 remained stable, exhibiting a C_α RMSD

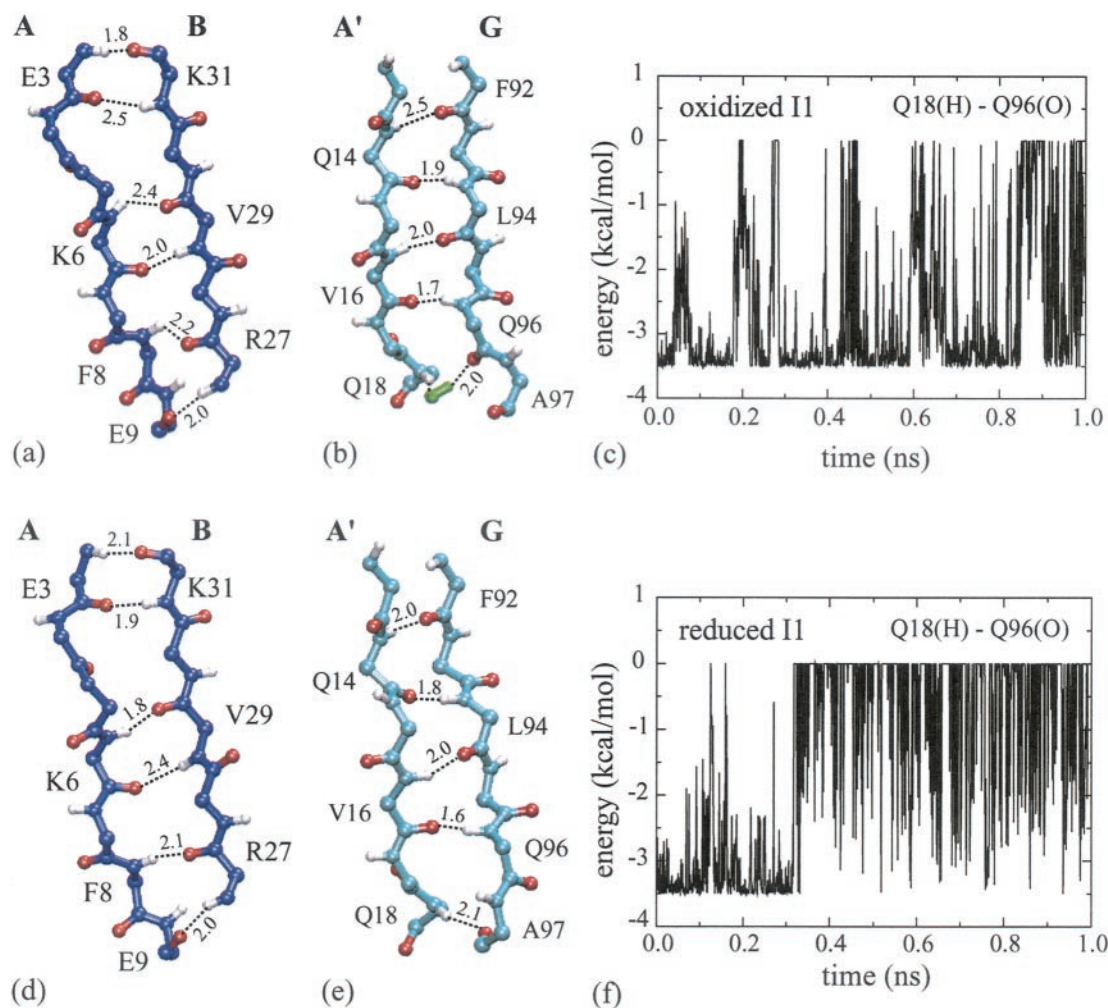


FIGURE 3 Structure and stability of interstrand hydrogen bonds in I1. Shown are hydrogen bonds between β -strands A, B, A' and G of oxidized (*a,b*) and reduced I1 (*d,e*) at the end of the 1 ns equilibration, together with the hydrogen bond energy fluctuations of Gln¹⁸(H)-Gln⁹⁶(O) during the equilibration of oxidized (*c*) and (*d*) reduced I1. The distances between oxygen (*red*) and hydrogen (*white*) of hydrogen bonds are given in Å. Other backbone atoms are shown in *blue* (A-, B-strands) and *cyan* (A'-, G-strands). A water molecule is shown in *green*. Hydrogen bonds are represented as *black dashed lines*.

from the crystal structure of <1.25 Å and an all-atom RMSD of <2.0 Å. The backbone hydrogen bonding structures between A- and B-strands and between A'- and G-strands at the end of the equilibration are shown in Fig. 3. Except for the bond Q18(H)-Q96(O), all six A-B backbone hydrogen bonds, E3(O)-K31(H), E3(H)-K31(O), K6(O)-V29(H), K6(H)-V29(O), F8(H)-R27(O) and E9(O)-R27(H), and four A'-G bonds, Q14(H)-F92(O), Q14(O)-L94(H), V16(H)-L94(O), V16(O)-Q96(H), remained stable, i.e., these hydrogen bonds occasionally broke, but reformed quickly. Hydrogen bond Q18(H)-Q96(O), the A'-G hydrogen bond nearest to the C-terminus, appears to be weak. During the equilibration of oxidized I1, polar residues Q18 and Q96 continuously suffered from attacks by surrounding water molecules. As a result, the bond Q18(H)-Q96(O) was found to have been dissociated and reformed several times, reflected in the hydrogen bond energy fluctuations shown in

Fig. 3 *c*. At the end of the equilibration Q18(H) and Q96(O) form hydrogen bonds with solvent water (Fig. 3 *b*). During the equilibration of reduced I1, Q18(H) broke up with its bond partner Q96(O) at 310 ps (Fig. 3 *f*), forming a new hydrogen bond with A97(O) (Fig. 3 *e*). The formation of this bond resulted in a more compact domain. The length of the reduced I1 module, defined as the distance between the two terminal C $_{\alpha}$ atoms, is 2 Å shorter than that of oxidized I1. However, the Q18(H)-A97(O) bond is easily broken under forces as small as 50 pN, leading to an additional extension of 2 Å as discussed below.

Constant velocity unfolding

The results of forced unfolding of both oxidized and reduced I1 domains with constant velocities of 0.1 Å/ps and

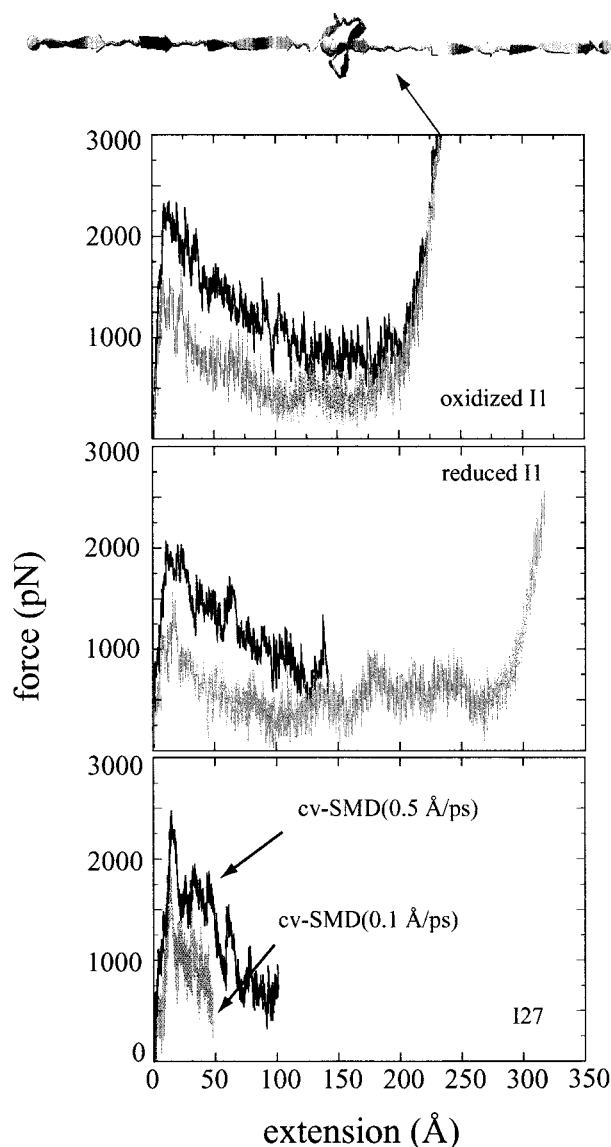


FIGURE 4 Force-extension profiles from constant velocity SMD simulations. Results from cv-SMD (0.5 Å/ps) (black) and cv-SMD(0.1 Å/ps) (red) are shown for both oxidized I1 (top), reduced I1 (middle), and I27 (bottom). The extension of oxidized I1 is restricted by the disulfide bond between β -strands C and E, as illustrated by the snapshot at ~ 220 Å extension (top).

0.5 Å/ps are compared in Fig. 4, together with results of unfolding I27. I1 domains exhibit a strong resistance against external forces in the extension range of 5–16 Å, a region broader than the major burst region of I27 of 12–15 Å (Lu et al., 1998). Overcoming the initial resistance of I1 domains requires slightly weaker forces than I27 at the same pulling speed. To unfold Ig domains at 0.5 Å/ps, for example, oxidized I1 requires a peak force of 2397 pN recorded at 10 Å extension; reduced I1 requires a peak force of 2090 pN at 11 Å extension; in contrast, I27 requires a stronger peak force of 2479 pN. Unfolding these domains at a

velocity of 0.1 Å/ps yields the same ordering of force peak values, but reduced by 20–30%. The lower peak forces required for unfolding I1 implies that I1 is slightly less stable than I27. Unraveling the module to extensions beyond the main force peak, which corresponds to the unfolding barrier, requires weaker and weaker forces until the domain is fully extended when forces rise again. Since oxidized I1 contains a disulfide bond, the domain can only extend to ~ 220 Å as shown in Fig. 4, whereas reduced I1 can be stretched to ~ 300 Å, the length of the completely extended I1 domain.

What conformational changes of I1 domains can be related to the main peak forces? For both I1 domains, the peak force coincides with a burst of backbone hydrogen bonds between β -strands A and B and between β -strands A' and G, as illustrated in Fig. 5 through the snapshots from cv-SMD (0.1 Å/ps) simulations. In these simulations, the disruption of backbone hydrogen bonds started from a pair of bonds near the N-terminus, between Glu³ on β -strand A and Lys³¹ on β -strand B. For example, during the unfolding of oxidized I1, a peak force of 1600 pN was encountered at 100 ps when two E3-K31 hydrogen bonds were seen to break (Fig. 5 a). Following this a second force peak of 1677 pN, measured at 168 ps, preceded the rupture of the remaining four A-B backbone hydrogen bonds at 170 ps and of four A'-G hydrogen bonds at 182 ps (Fig. 5 b,c). The extensions connected with the rupture of these bonds are 14 Å and 16 Å. Unfolding of reduced I1 exhibits the same sequence of ruptures of interstrand A-B and A'-G hydrogen bonds. The peak force of 1655 pN was found to follow the disruption of four A-B hydrogen bonds at 159 ps and to precede the rupture of four A'-G hydrogen bonds. Reduced I1 has one more A'-G backbone hydrogen bond, Q18(H)-A97(O). This bond broke within the first 50 ps when the C-terminus was straightened and the bond did not contribute to the major force peaks. During the disruption of A-B and A'-G hydrogen bonds, the secondary structure of the remaining part of the module were maintained. After the burst of A-B and A'-G hydrogen bonds, the module gradually lost its secondary structure by separating β -strands. The force peaks beyond the main reaction region from 5 Å to 16 Å extension are due to disruption of packing interactions and zipper-like unraveling of individual backbone hydrogen bonds.

Constant force unfolding

Constant forces of 50, 200, 650, and 750 pN have been applied to the I1 domain. Fig. 6 and Table 1 compare the extension of reduced I1 and I27 at forces of 50 pN and 200 pN for up to 10 ns. Under 50 pN the extension of I1 fluctuated between 1 Å to 3 Å, corresponding to the disruption (Fig. 6a) and re-formation of the hydrogen bond Q18(H)-A97(O) near the C-terminus. Applying a stronger force of 200 pN prohibited the reformation of this bond and

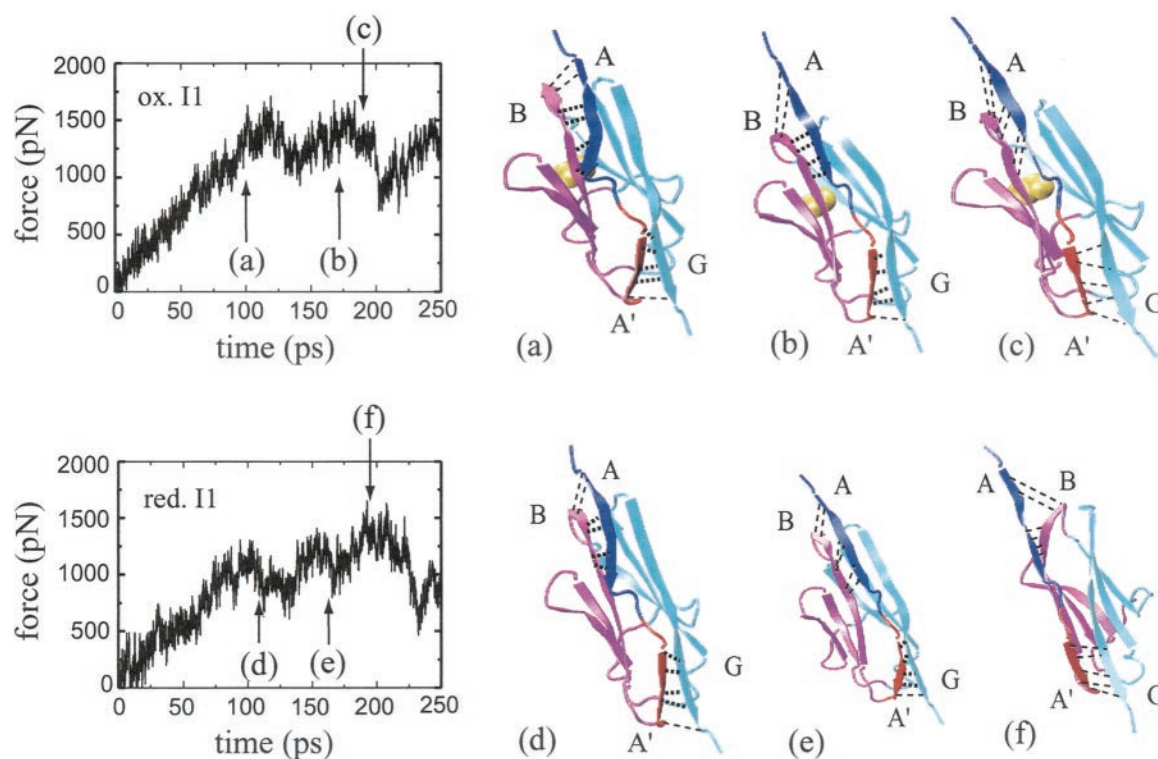


FIGURE 5 Representative force versus time curves (*left*) during early stages of cv-SMD($0.1\text{\AA}/\text{ps}$) simulations and snapshots of key events (*a-f*). The results for oxidized and reduced I1 domains are shown at the *top* and *bottom*, respectively. *Arrows* mark the instances when the corresponding snapshots were taken. (*a*) At 100 ps and extension of 7 \AA , a pair of backbone hydrogen bonds bridging Glu³ and Lys³¹ ruptures first. (*b*) The protein extends another 7 \AA and the remaining backbone hydrogen bonds between A- and B-strands break at 170 ps. (*c*) 12 ps later, four intact backbone hydrogen bonds between A'- and G-strands rupture at 16 \AA extension. The same order of hydrogen bond breaking occurs for reduced I1 at similar extensions (*d-f*). In all snapshots intact hydrogen bonds are represented as *thick black lines* while broken hydrogen bonds are shown as *thin lines*.

broke additionally two A-B hydrogen bonds between Glu³ and Lys³¹ at 5.7 ns (Fig. 6 *b*). However, the average extension of I1 increased only $\sim 2.0\text{\AA}$ from 2.0\AA at 50 pN to 4.3\AA at 200 pN, because the preserved other four hydrogen bonds between A- and B-strands prevented further extension. In comparison, titin I27 responded differently to the stretching forces. For a constant force of 50 pN the module appeared rigid with no rupture of any interstrand hydrogen bond observed (Fig. 6 *c*). As a result, the module experienced only a small extension of less than 1 \AA on average. Being stretched with a constant force of 200 pN, however, I27 extended up to 8 \AA , mainly due to the disruption of a pair of hydrogen bonds between A- and B-strands (Fig. 6 *d*). Re-formation of these two bonds at 9.18 ns resulted in an extension drop from over 7 \AA to less than 4 \AA . On average, the extension of I27 increased from 0.6\AA at 50 pN to 6.3\AA at 200 pN. Since this $\sim 6\text{\AA}$ elongation characterizes an I27 intermediate (Marszalek et al., 1999), which is associated with the unraveling of A-strand from B-strand, I1 seems unlikely to have a similar intermediate as I27 because the separation of its A-strand is prevented before crossing the main unfolding barrier and the 2 \AA change of extension prior to the barrier crossing is very small.

As the forces were increased, the breaking of all A-B and A'-G hydrogen bonds and separation of A- and A'-strands from the remaining fold were observed. Fig. 7 demonstrates that unfolding of the oxidized I1 domain happens in three key steps, discernible as three plateaus in the extension versus time curve observed during a cf-SMD (750pN) simulation. The three plateaus correspond to crossing barriers formed by backbone hydrogen bonds between A- and B-strands and between A'- and G-strands. Initially, the protein elongated 6 \AA from the equilibrium state to the first plateau at 120 ps. By disturbing the hydrophobic core and allowing water molecules to approach backbone oxygen and hydrogen atoms of residue Glu³ and Lys³¹, the two backbone hydrogen bonds between the two residues were weakened. At 420 ps the two bonds were disrupted, and water molecules formed new hydrogen bonds with oxygen and hydrogen atoms of Glu³ and Lys³¹, as shown in Fig. 7 *a*. The extension of the protein jumped 2 \AA entering the second plateau, which corresponded to climbing a barrier formed by the remaining four A-B backbone hydrogen bonds. At 585 ps, these bonds were broken accompanied by formation of hydrogen bonds with water molecules (Fig. 7 *b*). At this point, three A'-G backbone hydrogen bonds, Q14(H)-

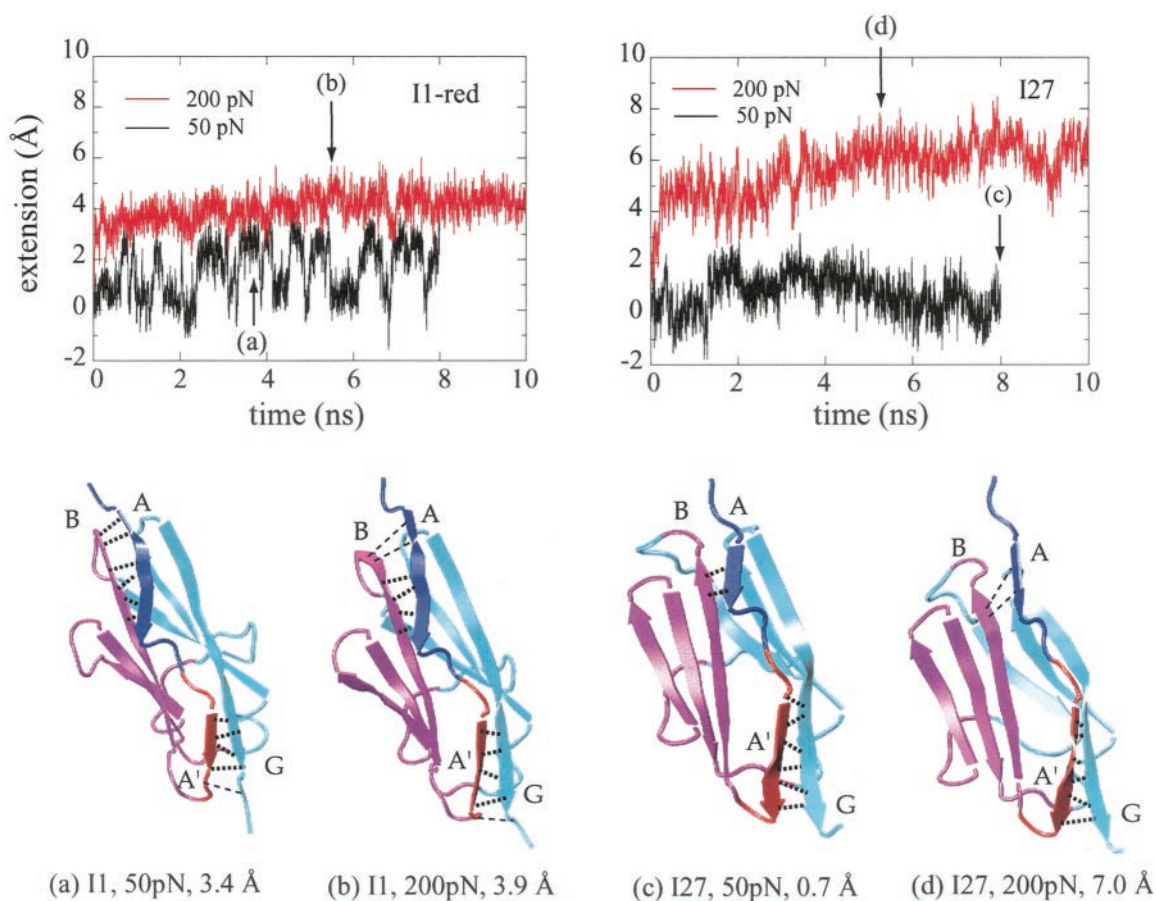


FIGURE 6 Extension-time profiles of reduced I1 (left) and I27 (right) for constant force of 50 pN and 200 pN, together with snapshots (a-d) of these two modules. (a) The extension fluctuation of I1 from 1 Å to 3 Å under 50 pN can be related to the rupture and re-formation of the hydrogen bond between Q18(H) and A97(O). (b) For a constant force of 200 pN two hydrogen bonds between Glu³ and Lys³¹ of I1 broke at 5.7 ns, but this rupture only led to an additional extension of less than 2 Å. (c) Extension of I27 fluctuated around 1 Å for a constant force of 50 pN. (d) For a constant force of 200 pN I27 elongated 6 Å further by disrupting the two A-B hydrogen bonds.

F92(O), Q14(O)-L94(H), and V16(H)-L94(O), were still intact (Fig. 7 c), whereas the other two A'-G bonds, i.e., those near the C-terminus, were already broken. The protein subsequently reached the third plateau, fluctuating between 12 Å and 16 Å. At the end of the plateau around 1140 ps, all five hydrogen bonds between A'- and G-strands were found broken, forming new hydrogen bonds with surrounding water molecules as shown in Fig. 7 d.

An analysis of the A-B interstrand hydrogen bond energy during the cf-SMD (750pN) simulation of oxidized I1 is

TABLE 1 Extension of titin domains from their equilibrated structures at constant forces of 50 pN and 200 pN

Titin domains	Extension (Å)	
	50 pN	200 pN
Reduced I1	2.0 ± 2.0	4.3 ± 2.0
I27	0.6 ± 2.0	6.3 ± 2.3

Extensions were calculated as the average of the extension during the last 4 ns of simulations.

provided in Fig. 8. Prior to the stretching, the equilibrated I1 domain has six interstrand hydrogen bonds between its A- and B-strands, as shown in Fig. 8. Upon stretching, two hydrogen bonds between E3 and K31 broke first. This pair of bonds, functioning like a “lock” to protect the integrity of the I1 domains, was also observed to be the first hydrogen bonds broken in all other cf-SMD simulations with forces higher than 650 pN. As shown in Fig. 8, bonds E3(H)-K31(O) and E3(O)-K31(H) were destabilized at 100 ps and 70 ps, respectively, with an energy jump from -3.5 kcal/mol to -1 kcal/mol. Fluctuating with an energy around -1.0 kcal/mol for about 350 ps, both bonds were completely broken at 420 ps. The remaining four A-B hydrogen bonds, K6(O)-V29(H), K6(H)-V29(O), F8(H)-R27(O), and E9(O)-R27(H), remained intact until 540 ps and were completely ruptured at ~600 ps, as shown in Fig. 7 b.

The reduced I1 domain exhibits the same sequence of hydrogen bond ruptures during SMD simulations as oxidized I1. The absence of the disulfide bond between two β-sheets, however, reduces the mechanical stability of the

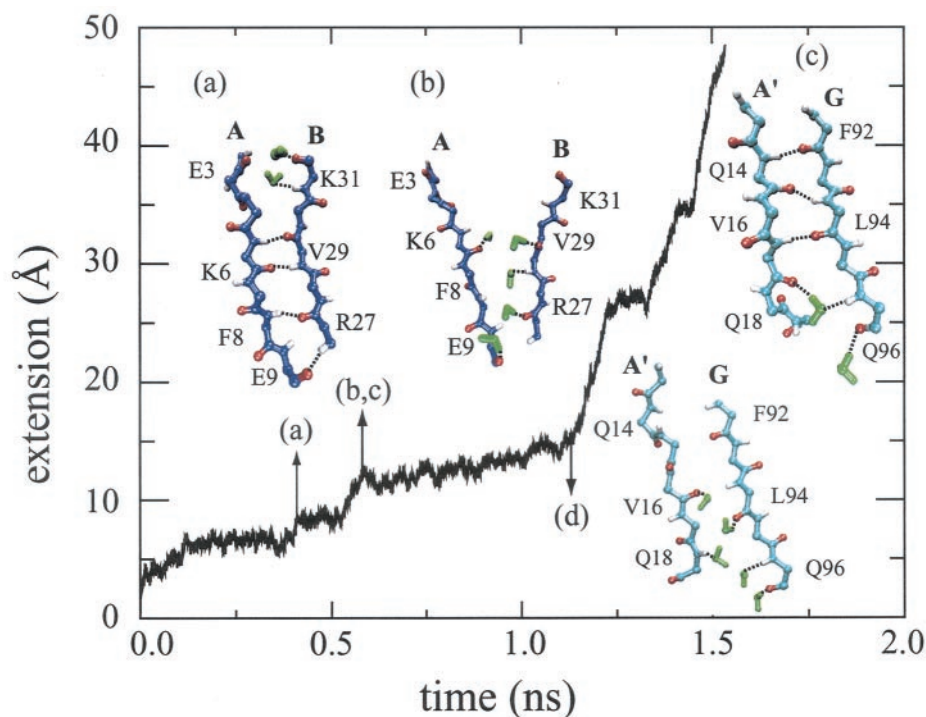


FIGURE 7 Force-extension profile and snapshots (*a-d*) of key events from a cf-SMD(750pN) simulation of the oxidized I1 domain. (*a*) Two backbone hydrogen bonds between A- and B-strands broke at 410 ps. (*b*) The remaining four A-B hydrogen bonds broke at 585 ps. (*c*) Two interstrand hydrogen bonds between A'- and G-strands broke at 585 ps, followed (*d*) by the rupture of the remaining three bonds at 1110 ps.

module. Fig. 9 shows a comparison of the results from SMD simulations of oxidized and reduced I1 domains for forces of 650 pN and 750 pN. Three transition states can be identified in Fig. 9 as plateaus or shoulders in extension-time profiles from SMD simulations. Similar to unfolding oxidized I1 analyzed above, the first plateau at ~ 5 Å, shown in Fig. 9, corresponds to disrupting the hydrophobic core and overcoming the resistance imposed by A-B backbone hydrogen bonds, especially between residue E3 and K31. The second plateau/shoulder, corresponding to the separation of A-strand from B-strand, are generally short and were found at an extension of ~ 9 Å for oxidized I1, and of 11 Å for reduced I1. Oxidized I1 turns out to be more stable than reduced I1 when one compares the third plateau/shoulder, which corresponds to disturbing the four A'-G backbone hydrogen bonds. A constant force of 650 pN could not separate A'-strand from G-strand of oxidized I1 within 2.5 ns, whereas for reduced I1 the A'-strand was peeled away from the G-strand by the same force after the rupture of the A'-G hydrogen bonds at 2.1 ns. The results suggest that the disulfide bond enhances the stability of oxidized I1 by restricting the disruption of backbone hydrogen bonds between A'- and G-strands.

CONCLUSIONS AND OUTLOOK

I1 and I27 are homologous modules with the same β -sandwich architecture. SMD simulations of I1 show that the

main mechanical resistance to an external force occurs within the initial 16 Å extension and arises mainly from its interstrand hydrogen bonding between A-B and A'-G strands. The force peaks observed in constant velocity pulling simulations (Fig. 5) or the plateaus observed in constant force pulling simulations (Fig. 7), corresponding to crossing the barrier that separates folded and unfolded states, coincide with the breaking of A-B and A'-G hydrogen bonds. Since I1 modules encounter the unfolding barrier very early, namely at extension of ~ 5 Å, it is likely that the transitional state of unfolding I1 is close to its native state. After the rupture of the two clusters of hydrogen bonds and separation of the A- and A'-strands, the remaining interstrand backbone hydrogen bonds are easily ruptured by “unzipping.” These observations are similar to what has been reported from SMD simulations of I27 (Lu et al., 1998; Lu and Schulten, 1999, 2000; Marszalek et al., 1999).

Although the general unfolding pathways of I1 and I27 are similar, the modules exhibit a different mechanical design in terms of A-B and A'-G backbone bonding structure and the presence of a disulfide bridge, leading to different mechanical responses upon stress. First, the mechanical stability of I1 is largely due to the six backbone hydrogen bonds between its A- and B-strands, not the A'-G hydrogen bonds as for I27. This is because I1 has a larger number of hydrogen bonds between A- and B-strands than of hydrogen bonds between A'- and G-strands. Second, the mechanical stability of I1 domains is slightly less than that

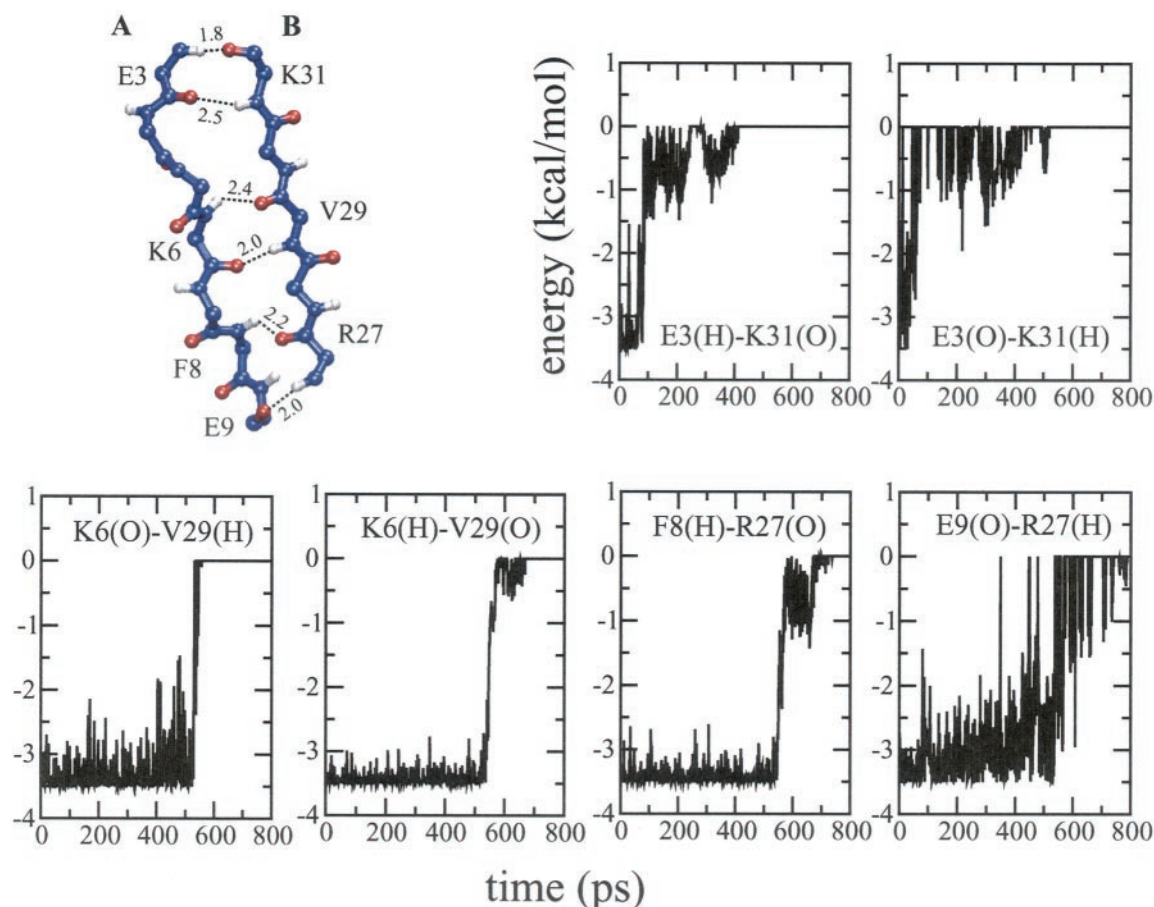


FIGURE 8 Energy analysis of six backbone hydrogen bonds between A- and B-strands during a cf-SMD (750pN) simulation of oxidized I1. The equilibrated structure of β -strands A and B are shown at *top left*. The energy versus time profiles for individual bonds reveal that the interstrand hydrogen bonds rupture in two steps. Two of them, between Glu³ and Lys³¹ (*top right*), broke earlier than the other four bonds (*bottom*). The latter four bonds broke concurrently at \sim 580 ps.

of I27, as reflected in the maximum unfolding force shown in Fig. 4. The main reason is that in I1 domains no more than four backbone hydrogen bonds break concurrently during stretching (six A-B bonds break in two steps: two bonds break first, followed by the break of the remaining four bonds), which contribute to the force peaks recorded in simulations; in contrast, I27 has six A'-G backbone hydrogen bonds that break simultaneously (Lu et al., 1998). Comparison of the extension of I1 and I27 at forces of 50 and 200 pN (Table 1) leads to a third difference. I27 exhibits an \sim 6 Å extension "hump" revealed in force-extension curves (Marszalek et al., 1999). I1 domains, however, should not exhibit such hump at forces up to 200 pN because of the large number of A-B interstrand hydrogen bonds. A fourth difference between I1 and I27 is due to the disulfide bond. Our simulations of oxidized and reduced I1 revealed that the disulfide bridge between Cys³⁶ and Cys³¹ increases the mechanical stability and limits the extension of I1 within 220 Å. Indeed, reduced spacing between force peaks has been observed in unfolding oxidized I1 (J. Fernandez, personal communication).

Limited by current available computational resources, the timescale accessible to SMD simulations, i.e., nanosecond, is six orders of magnitude shorter than the millisecond timescale over which titin modules are stretched and unfolded in AFM experiments. This timescale gap requires a pulling velocity used in SMD simulations about six order of magnitude faster than in experiments, leading to a discrepancy in the unfolding forces as discussed previously (Izrailev et al., 1997; Lu and Schulten, 1999). This problem may be solved in the future with simulations applying reduced pulling speeds close to experimental values, requiring, however, vastly improved computational resources.

Nevertheless, the hypothesis suggested by our SMD simulations that hydrogen bonds protect Ig domains is worth experimental examination. For example, I27 mutants in which either A-B or A'-G hydrogen bonds were disrupted have been engineered and stretched with AFM after suggestions derived from SMD simulations (Marszalek et al., 1999; Li et al., 2001b). Disrupting A-B hydrogen bonds of I27 through mutation eliminates the pre-burst intermediate (Marszalek et al., 1999). Mutating residues involving A'-G

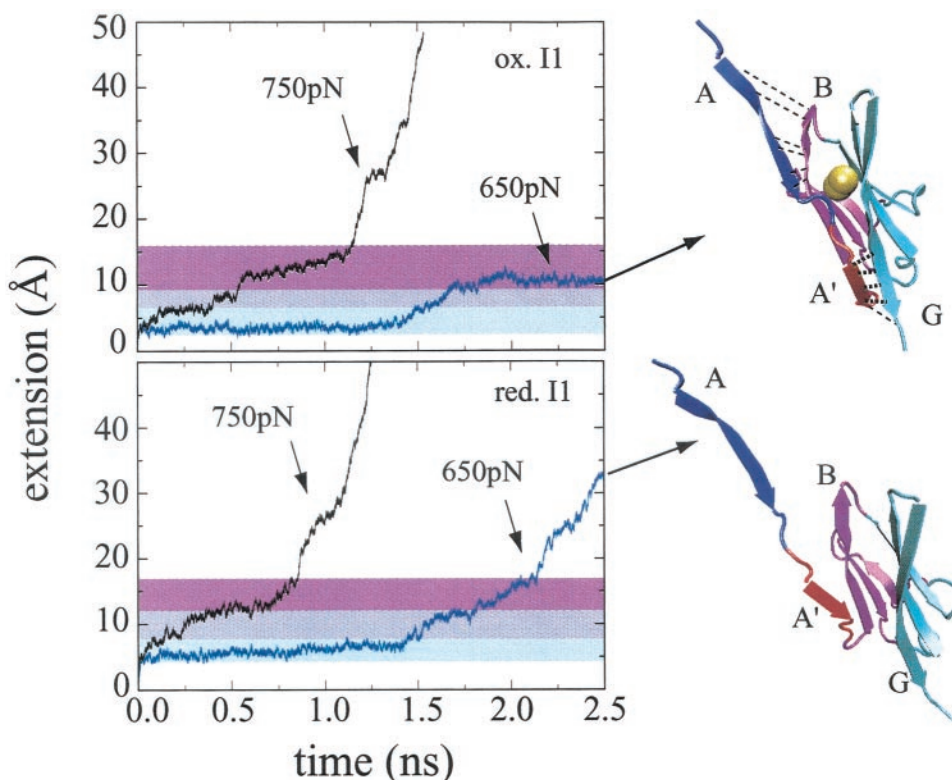


FIGURE 9 Representative extension-time profiles from cf-SMD simulations of oxidized (*top*) and reduced I1 (*bottom*). The snapshots of I1 domains at the end of the simulations are shown on the *right*. The *shaded areas* in profiles correspond to key transition states for crossing barriers formed by hydrogen bonds: Glu³-Lys³¹ hydrogen bond rupture (*cyan*); rupture of the remaining bonds bridging A- and B-strands (*light purple*); rupture of the bonds between A'- and G-strands (*purple*).

hydrogen bonds produced proteins that require weaker unfolding forces than wild type I27 (Li et al., 2001b). A similar approach may be applied to I1. For example, by mutating residue K6 to proline reduces the number of A-B hydrogen bonds, and, correspondingly, separation of the A-strand should occur at weaker forces. AFM stretching of this mutant may even produce a pre-burst “hump,” corresponding to A-strand separation before the burst of A'-G backbone hydrogen bonds.

New structures of Ig domains will likely be solved in the near future, providing further opportunities to compare their mechanical responses to AFM generated force and simulated force, as well as to develop an understanding of the evolutionary design and function of the remarkable protein titin.

This work was supported by National Institutes of Health Research Grants PHS5P41RR05969 and 1R01GM60946 and National Science Foundation supercomputer time grant NRAC MCA93S028.

REFERENCES

Brünger, A. T. 1992. X-PLOR, Version 3.1: A System of X-ray Crystallography and NMR. The Howard Hughes Medical Institute and Department of Molecular Biophysics and Biochemistry, Yale University.

Carrion-Vazquez, M., A. Oberhauser, S. Fowler, P. Marszalek, S. Broedel, J. Clarke, and J. Fernandez. 1999. Mechanical and chemical unfolding of a single protein: a comparison. *Proc. Natl. Acad. Sci. U.S.A.* 96: 3694–3699.

Consortium, 2001. Initial sequencing and analysis of the human genome. *Nature*. 409:860–921.

Erickson, H. 1994. Reversible unfolding of fibronectin type III and immunoglobulin domains provides the structural basis for stretch and elasticity of titin and fibronectin. *Proc. Natl. Acad. Sci. U.S.A.* 91: 10114–10118.

Erickson, H. 1997. Stretching single protein modules: titin is a weird spring. *Science*. 276:1090–1093.

Freiburg, A., K. Trombitas, W. Hell, O. Cazorla, F. Fougereuse, T. Centner, B. Kolmerer, C. Witt, J. Beckmann, C. Gregorio, H. Granzier, and S. Labeit. 2000. Series of exon-skipping events in the elastic spring region of titin as the structural basis for myofibrillar elastic diversity. *Circ. Res.* 86:1114–1121.

Gao, M., H. Lu, and K. Schulten. 2001. Simulated refolding of stretched titin immunoglobulin domains. *Biophys. J.* 81:2268–2277.

Granzier, H., M. Helmes, and K. Trombitas. 1996. Nonuniform elasticity of titin in cardiac myocytes: a study using immunoelectron microscopy and cellular mechanics. *Biophys. J.* 70:430–442.

Granzier, H., and S. Labeit. 2002. Cardiac titin: an adjustable multifunctional spring. *J. Physiol.* 541:335–342.

Humphrey, W., A. Dalke, and K. Schulten. 1996. VMD—visual molecular dynamics. *J. Mol. Graphics.* 14:33–38.

Isralewitz, B., M. Gao, and K. Schulten. 2001. Steered molecular dynamics and mechanical functions of proteins. *Curr. Opin. Struct. Biol.* 11: 224–230.

- Izrailev, S., S. Stepaniants, M. Balsera, Y. Oono, and K. Schulten. 1997. Molecular dynamics study of unbinding of the avidin-biotin complex. *Biophys. J.* 72:1568–1581.
- Jorgensen, W. L., J. Chandrasekhar, J. D. Madura, R. W. Impey, and M. L. Klein. 1983. Comparison of simple potential functions for simulating liquid water. *J. Chem. Phys.* 79:926–935.
- Kalé, L., R. Skeel, M. Bhandarkar, R. Brunner, A. Gursoy, N. Krawetz, J. Phillips, A. Shinozaki, K. Varadarajan, and K. Schulten. 1999. NAMD2: greater scalability for parallel molecular dynamics. *J. Comp. Phys.* 151:283–312.
- Kellermayer, M., S. Smith, H. Granzier, and C. Bustamante. 1997. Folding-unfolding transition in single titin modules characterized with laser tweezers. *Science.* 276:1112–1116.
- Klimov, D. K., and D. Thirumalai. 1999. Stretching single-domain proteins: phase diagram and kinetics of force-induced unfolding. *Proc. Natl. Acad. Sci. U.S.A.* 96:1306–1315.
- Klimov, D. K., and D. Thirumalai. 2000. Native topology determines force-induced unfolding pathways in globular proteins. *Proc. Natl. Acad. Sci. U.S.A.* 97:7254–7259.
- Li, H., C. V. Mariano, A. F. Oberhauser, P. E. Marszalek, and J. M. Fernandez. 2001b. Point mutations alter the mechanical stability of immunoglobulin modules. *Nature Struct. Biol.* 7:1117–1120.
- Li, H. B., A. F. Oberhauser, S. B. Fowler, J. Clarke, and J. M. Fernandez. 2000. Atomic force microscopy reveals the mechanical design of a modular protein. *Proc. Natl. Acad. Sci. U.S.A.* 97:6527–6531.
- Li, H., A. F. Oberhauser, S. D. Redick, M. Carrion-Vazquez, H. Erikson, and J. M. Fernandez. 2001a. Multiple conformations of PEVK proteins detected by single-molecule techniques. *Proc. Natl. Acad. Sci. U.S.A.* 98:10682–10686.
- Linke, W. A. 2000. Stretching molecular springs: elasticity of titin filaments in vertebrate striated muscle. *Histol. Histopathol.* 15:799–811.
- Linke, W. A., M. Ivemeyer, P. Mundel, M. R. Stockmeier, and B. Kolmerer. 1998. Nature of PEVK-titin elasticity in skeletal muscle. *Proc. Natl. Acad. Sci. U.S.A.* 95:8052–8057.
- Linke, W. A., D. E. Rudy, T. Centner, M. Gautel, C. Witt, S. Labeit, and C. C. Gregorio. 1999. I-band titin in cardiac muscle is a three-element molecular spring and is critical for maintaining thin filament structure. *J. Cell Biol.* 146:631–644.
- Lu, H., B. Israelewitz, A. Krammer, V. Vogel, and K. Schulten. 1998. Unfolding of titin immunoglobulin domains by steered molecular dynamics simulation. *Biophys. J.* 75:662–671.
- Lu, H., and K. Schulten. 1999. Steered molecular dynamics simulation of conformational changes of immunoglobulin domain I27 interpret atomic force microscopy observations. *Chem. Phys.* 247:141–153.
- Lu, H., and K. Schulten. 2000. The key event in force-induced unfolding of titin's immunoglobulin domains. *Biophys. J.* 79:51–65.
- Ma, K., L. Kan, and K. Wang. 2001. Polyproline II helix is a key structural motif of the elastic PEVK segment of titin. *Biochemistry.* 40:3427–38.
- MacKerell Jr., A. D., D. Bashford, M. Bellott, R. L. Dunbrack Jr., J. Evanseck, M. J. Field, S. Fischer, J. Gao, H. Guo, S. Ha, D. Joseph, L. Kuchnir, K. Kuczera, F. T. K. Lau, C. Mattos, S. Michnick, T. Ngo, D. T. Nguyen, B. Prodhom, I. W. E. Reiher, B. Roux, M. Schlenkrich, J. Smith, R. Stote, J. Straub, M. Watanabe, J. Wiorkiewicz-Kuczera, D. Yin, and M. Karplus. 1998. All-hydrogen empirical potential for molecular modeling and dynamics studies of proteins using the CHARMM22 force field. *J. Phys. Chem. B.* 102:3586–3616.
- Marszalek, P. E., H. Lu, H. Li, M. Carrion-Vazquez, A. F. Oberhauser, K. Schulten, and J. M. Fernandez. 1999. Mechanical unfolding intermediates in titin modules. *Nature.* 402:100–103.
- Maruyama, K. 1997. Connectin/titin, a giant elastic protein of muscle. *FASEB J.* 11:341–345.
- Mayans, O., J. Wuerges, S. Canela, M. Gautel, and M. Wilmanns. 2001. Structural evidence
- Tskhovrebova, L., J. Trinick, J. Sleep, and R. Simmons. 1997. Elasticity and unfolding of single molecules of the giant protein titin. *Nature.* 387:308–312.
- Wang, K. 1996. Titin/connectin and nebulin: giant protein ruler of muscle structure and function. *Adv. Biophys.* 33:123–134.